Hindawi
Advances in Civil Engineering
Volume 2023, Article ID 3493396, 19 pages
https://doi.org/10.1155/2023/3493396

Research Article

Assessing 3D Seismic Plastic Damages of Arch Dams Considering Optimum Mesh Spaces Based on FOS Analyses and 2023 Kahramanmaraş, Hatay, Malatya, and Gaziantep Earthquakes in Turkey

Murat Cavuslu and Emrah Dagli

Department of Civil Engineering, Zonguldak Bülent Ecevit University, 67600 Zonguldak, Turkey

Correspondence should be addressed to Murat Cavuslu; murat.cavusli@beun.edu.tr

Received 30 March 2023; Revised 14 June 2023; Accepted 15 June 2023; Published 5 July 2023

Academic Editor: Jiang Hu

In this paper, the three-dimensional (3D) seismic plastic damage performance of the Ermenek Arch Dam (220 m), which was built in Karaman, Turkey, in 2009, is investigated by including different gallery spaces. 3D modeling of the dam is performed using the finite-difference method, and four various gallery spaces are added to the dam model considering their original oval geometries. WIPP-Drucker (WD) material model is utilized for the dam's concrete material in creep and seismic damage analyses. Moreover, the Mohr–Coulomb material model is utilized for the foundation. Quiet nonreflecting and free-field boundary conditions are taken into account in the earthquake analyses, and reflecting (fix) boundary condition is used in the factor of safety (FOS) analyses in order to minimize the reflection of earthquake waves at the boundaries. First, the FOS analyses of the Ermenek Dam are performed considering the WD material model, and the optimum mesh space is determined according to FOS analyses. Then, 3D earthquake analyses are performed for 10 important strong ground motions that occurred in Kahramanmaraş, Hatay, Malatya, and Gaziantep in 2023. As a result of the FOS analyses, it is suggested that the mesh length of arch dams should not be chosen randomly while performing the earthquake analyses, and the FOS analyses of arch dams should be carried out using the WD material model before choosing the mesh space. Besides, it is concluded that selected ground motions for seismic analyses have created significant plastic damage around the galleries of the Ermenek Arch Dam, and gallery spaces are of great importance for the seismic plastic damage behavior of arch dams.

1. Introduction

Water is of great importance for human life, and the dams are constructed to make maximum usage of the water. Many types of dams have been built from the past to today. Arch dams are one of the most significant dam types. These dams are constructed using concrete material, and they are geometrically different from other dam types. Since arch dams have high and oval geometry, these dams are preferred in basins where the water level is high. For this reason, examining the seismic and crack response of arch dams is crucial for the future of people and living things. Arch dams have always attracted the attention of researchers from past to present, and they have been the research subject of many researchers. Hamidian and Seyedpoor examined the critical design of concrete arch dams. A procedure was asserted to model the optimal geometrical shapes of arch dams considering dam–fluid interaction [1]. Sani and Lotfi [2] performed a new model technique to assess the dynamic response of the concrete arch dams. The ideal-coupled modal approach was proposed for the seismic analysis of concrete arc dams [2]. Bayraktar et al. [3] examined the effects of finite element model updates on determining the nonlinear earthquake response of arch dams. Berke Arch Dam was selected for numerical modeling, and the arch dam–foundation-reservoir interaction was modeled by the Lagrangian approach. According to experimental and numerical test results, maximum principal stresses were observed on the right and left sides of

the dam [3]. Alembagheri and Ghaemian examined the nonlinear incremental seismic analyses of concrete arch dams. In total, 12 various earthquakes were utilized in the seismic analyses. According to numerical analyses, it was determined that the proposed limit-states could be used in the earthquake vulnerability analyses of an arch dam [4]. Wang et al. [5] researched the seismic response of arch dams taking into account the interaction behavior. Various important factors, such as the earthquake's mechanism, block shape, and water level, are further considered to analyze their impact on the failure response of the dam. The earthquake analyses showed that the earthquake variation may be the most significant factor for the dams in terms of the damage response [5]. Tarinejad et al. [6] evaluated the earthquake response of arch dams taking into account nonuniform ground motions created by an earthquake wave scattering model. It was observed that nonuniform and uniform earthquakes create very different earthquake effects on the concrete body of the arch dam [6]. Hariri-Ardebili and Kianoush [7] examined the calibration procedure and nonlinear seismic response of high arch dams. It was concluded that thermal differences have a crucial effect on the static response of thin high-arch dams and should be taken into account for the calibration process [7]. Zhang et al. [8] examined the structural behavior of a high arch dam exposed to an underwater explosion shock. It was concluded that each monolith became more independent, and the entire dam structure was more flexible due to the shear key failures [8]. Wang et al. [9] examined the earthquake fragility of an arch dam (210 m) using seismic damage analysis models. Analysis results showed that the arch dams might be seriously damaged by strong earthquakes when varying material parameters and ground motions are considered [9]. Ma et al. [10] investigated the displacements and principal stresses under various load combinations, such as normal load and special load, for the Xiulodu Arch Dam with a finite element program. Cracking performances of dam were also evaluated in overload and water load conditions. Results indicated that the symmetry and uniformity seemed to be similar for displacement for different working conditions. Abutment rock mass under normal load conditions produced very small tensile damage, while it needed to be reinforced for overload conditions [10]. Du et al. [11] proposed an analyzing method that benefits the modeling of the initial static behavior of the Xiaowan Arch Dam. The seismic behavior of dam was also performed by taken into account the energy dispersion, and this made approximately 20%–40% reduction on stresses [11]. Wieland and Kirchen [12] observed the Punt dall Gall Arch Dam in a long period of time with considerations of maximum displacements, cracks in galleries, water, and temperature effects by installing necessary equipment. Seismic behaviors were also monitored with ground motion instruments [12]. Song et al. [13] performed a nonlinear finite element analysis, including a deformation reinforcement model for the Baihetan Dam and geomechanic test. Nonsymmetrical deformations on dam were also considered. Positive effects of modification of the slenderness ratio on dam safety analysis were clearly seen [13]. Zelin et al. [14] simulated the Lizhou Arc Dam with finite element method (FEM) software to investigate the stability. Geo-mechanical test was also carried out to verify the shear zones effect on dam abutment as seen in FEM analysis. Safety calculations for the dam emphasized that an overload coefficient of 1.4–2.2 caused no apparent cracks, while the cracks spread almost the whole part when the coefficient reached to 6.3–6.6 [14]. Chen et al. [15] performed an analysis to define the earthquake behavior of the Baihetan Arch Dam with dynamic analysis method. Damages were observed with a proposed, including the ratio of monolith damaged area and volume. Results showed that damage of monolith enhanced enormously when peak ground accelerations (PGA) is between 0.4 and 0.6 g, and it might be a good indicator of damage situation [15]. Zhang and Zhang [16] applied a new method of analysis to define the seismic failure mechanism with a distinct element code program. The suggested model includes the effect of coupling the dam–foundation–reservoir system, energy dissipation, and nonlinear contact. Earthquake behavior of the Chinese national dam exposed to strong ground motion was analyzed with this methodology. The condition that overload <3.7 had a relatively small displacement effect on dam, while the integrity of dam began to lose when the overload reached 5.7 [16]. Fu et al. [17] examined the effect of high uplift pressures on the Huaguangtan Dam with a finite element program. Video tests on boreholes were executed in order to observe this uplift pressure on-site and possible damages on the dam. Results of the study emphasized that even at high uplift pressure had dam's safety were not affected significantly [17]. Pan et al. [18] investigated the earthquake behavior on dam–foundation system for the Baihetan Dam. Factor of safety (FOS) for the dam against sliding was also evaluated, and even ground motion that occurred on dam did not reduce the FOS value under 1 [18]. Luo et al. [19] analyzed the Xiluodu Dam using the FEM and measurements. Hydrostatic load and water level effect on the deformation, displacement, and stress characteristics of dam were observed. Results indicated that the stress and strain results of FEM analysis were compatible with field measurements. Hydrostatic load also had significant eff ects [19]. Chen et al. [20] suggested a model test to simulate the similarity of cracking for induced joints. This simulation caused a reduction on tensile stresses. Toughness of fracture and intensity factor of stress were analyzed for the Shapai RCC Arch Dam [20]. Zacchei et al. [21] performed FEM and gravity method analyses on the Rules Arch Dam to observe the effect of both structure–fluid–foundation interaction and earthquake. Dynamic stresses were computed both with empty and full reservoir conditions. Modeling and field observations were in good agreement with each other [21]. Alcay et al. [22] researched the effect of temperature and water loads on the displacement behavior of the Ermenek Arch Dam, and they were observed with monitoring of geodetic and pendulum on the field. The results obtained were compatible when compared to displacements obtained from geodetic and derived methods [22]. Wang et al. [23] developed a method of analysis to determine the earthquake behavior of the Pacoima Arch Dam. This method included the interaction of dam–water, contraction joints, cracking of earthquake damage, and reinforcing the concrete of dam. Damage observed from the actual earthquake seems to be similar with the results obtained from the proposed

method [23]. Pirooznia and Moradloo [24] examined the dynamic characteristics of the Morrow Point Arch Dam with consideration of the effect of loading rate and size. Stress and displacement values for both empty and full reservoir conditions showed that those values for all conditions were increased when considering an effect of size and loading rate [24]. Wu et al. [25] performed a FEM analysis for Xiaowan Dam and observed the in-situ data. Mechanisms of deformation modulus for reservoir basin bedrock were analyzed. The results showed that upstream range and depth of foundation had a significant effect on the deformation, but downstream had slight effect [25]. There are several studies on the arch dam's seismic behavior while observing the literature. However, there is no study in which the optimum mesh length for arch dams is found by considering the FOS analyses, and seismic plastic damages of arch dams are obtained considering the optimum mesh length and WIPP-Drucker (WD) material model. For this reason, this study is of great importance in terms of eliminating these deficiencies.

2. WD Creep Material Model

Modeling creep and the FOS response of concrete material is very important when the creep life of water structures is examined. In this paper, a special model is considered for modeling the arch dam's seismic safety and creep responses. The FLAC3D program is a specialized software designed for the design, analysis, and investigation of underground and surface structures and their structural behavior. It has a unique syntax and coding language. There are many material models in this program that researchers may not be aware of. These material models are similar to the material models found in the literature. Since this program is based on the finite-difference method, all material models in this program are also based on this method. Therefore, the material models used in this study demonstrate the fundamental characteristics of the finite-difference method. The use of these material models and material methods, which researchers may not be aware of, as alternative material models to other material models, are of great importance for evaluating the structural behavior of arch dams in this study. For this reason, the purpose of using the material models used in this study is to bring a new perspective to reveal the seismic behavior of arch dams. In addition, one of the most important aims of this study is to reveal the effects of this material model on the seismic behavior of arch dams. In FLAC software, the earthquake creep response of concrete materials can be modeled by combining the Drucker–Prager (DP) model with the WIPP viscoelastic model [26]. When material models in FLAC3D software are investigated, it is seen that the DP model is the most sufficient model with the WIPP model due to both material models being derived from the 2nd deviatoric stress tensor's invariant [26]. DP model and WIPP model depend on the radial distance from the isotropic-stress locus. The creep formulation in the DP material model is shown to be similar to the WIPP model [26]. The function of shear yield used in the WD material model is defined as follows:

$$f^s = \tau + q_\varphi \sigma_o - k_\varphi, \tag{1}$$

$f^s = 0$ at yield.

$$\sigma_o = \frac{\sigma_{kk}}{3}. \tag{2}$$

$$\tau = \sqrt{J_2}. \tag{3}$$

J_2: the 2nd deviatoric stress tensor's invariant, q_ϕ and k_ϕ are the properties of the material [26]:

$$J_2 = \frac{\sigma_{ij}^d \, \sigma_{ij}^d}{2}. \tag{4}$$

τ is the stress magnitude [26]:

$$\overline{\sigma} = \sqrt{\frac{\sigma_{ij}^d \, \sigma_{ij}^d}{2}}, \tag{5}$$

$$\overline{\sigma} = \sqrt{3}\tau. \tag{6}$$

g^s is defined as the plastic potential function that is almost similar to the function of yield except for the substitution of q_ψ for q_ϕ instead as a property of material controlling dilation [26]:

$$g^s = \tau + q_\psi \sigma_o. \tag{7}$$

If f^s is 0.

$$\in_{ij}^{\cdot dp} = \lambda \frac{\partial g^s}{\partial \sigma_{ij}^d}, \tag{8}$$

$$\in_{\circ}^{\cdot p} = \lambda \frac{\partial g^s}{\partial \sigma_{\circ}}. \tag{9}$$

λ is a multiplier, prepresents the plastic, and d symbolizes deviatoric [26]:

$$\in_{ij}^{\cdot dp} = \lambda \frac{\sigma_{ij}^d}{2\tau}, \tag{10}$$

$$\in_{\circ}^{\cdot p} = \lambda q_\psi. \tag{11}$$

Moreover, the WD model has a tensile yield surface, and the surface of tensile yield is shown below [26]:

$$f^t = \sigma_{\circ} - \sigma^t. \tag{12}$$

σ^t represents the strength of tensile yield, and the function of plastic potential is presented below [26]:

Figure 1: General view of Ermenek Arch Dam [27, 28].

$$g^t = \sigma_\circ. \tag{13}$$

The tensile yield's strain rates are shown below [26]:

$$\in_{ij}^{\cdot dp} = 0, \tag{14}$$

$$\in_{\circ}^{\cdot p} = \lambda. \tag{15}$$

λ is calculated from the situation where $f^t = 0$. Besides, the tensile strength must be maximum of $f^s = 0$. When both analyses of creep and plastic earthquake take place, it is presumed that the terms of associated strain rates act "in series" [26]:

$$\in_{ij}^{\cdot p} = \in_{ij}^{\cdot de} + \in_{ij}^{\cdot dv} + \in_{ij}^{\cdot dp}. \tag{16}$$

The terms shown above are strain rates of elastic, viscous, and plastic, respectively [26]:

$$\in_{ij}^{\cdot p} = \frac{\sigma_{ij}^{\cdot d}}{2G} + \frac{\sigma_{ij}^{\cdot d}}{2\overline{\sigma}} + \left(3\in^{\cdot} + \sqrt{3}\lambda\right). \tag{17}$$

The scheme of the creep solution can be extended to include plastic strain increments [26]. So,

$$\sigma_{ij}^{d^*} = \sigma_{ij}^{d^*} + 2G\Delta t\left[\in_{ij}^{\cdot d} - \frac{\sigma_{ij}^{d}}{2\sigma^{-}}\left(3\in^{\cdot} + \sqrt{3}\lambda\right)\right]. \tag{18}$$

3. General Information about Ermenek Arch Dam

Ermenek Dam is one of the longest concrete arch dams in the world. This dam is among the most special water structures built in the world in terms of body shape and height. The Ermenek Dam was built in 2009 in Karaman, Turkey, on the Göksu River (Figure 1) [27]. The construction period of the dam is 7 years in total. The dam is built on hard rocks and meets the electricity and irrigation needs of the people in the region at a high rate. The Poisson's ratio, mass density, and modulus of elasticity of the dam foundation are 0.22, 2,765 kg/m^3, and 43 GPa, respectively [27]. The body width of the dam is 150 m, and the length of the crest is 123 m. Moreover, the height of the dam from the foundation is 210 m. The reservoir area of the dam is 58 km^2, and the energy capacity of the dam is 1,047 W hr/year [27]. The dam body was constructed of concrete material, and the Poisson's ratio, mass density, and the modulus of elasticity of the concrete used for the construction of the dam are 0.24, 2,615 kg/m^3, and 32 GPa, respectively. Ermenek Dam was constructed close to the East Anatolian Fault (EAF). The EAF is one of the well-known strike-slip fault lines located in eastern Turkey. The EAF creates the tectonic boundary of transform type between the Anatolian Plate and the Arabian Plate moving in the northward direction. It has produced many important earthquakes in Turkey and caused many losses of life and property. The most important and the latest earthquakes produced by the EAF are the 2023 Kahramanmaraş, Hatay, Malatya, and Gaziantep earthquakes. This fault line produced Mw 7.7 and Mw 7.6 earthquakes in Kahramanmaraş with 9 hr

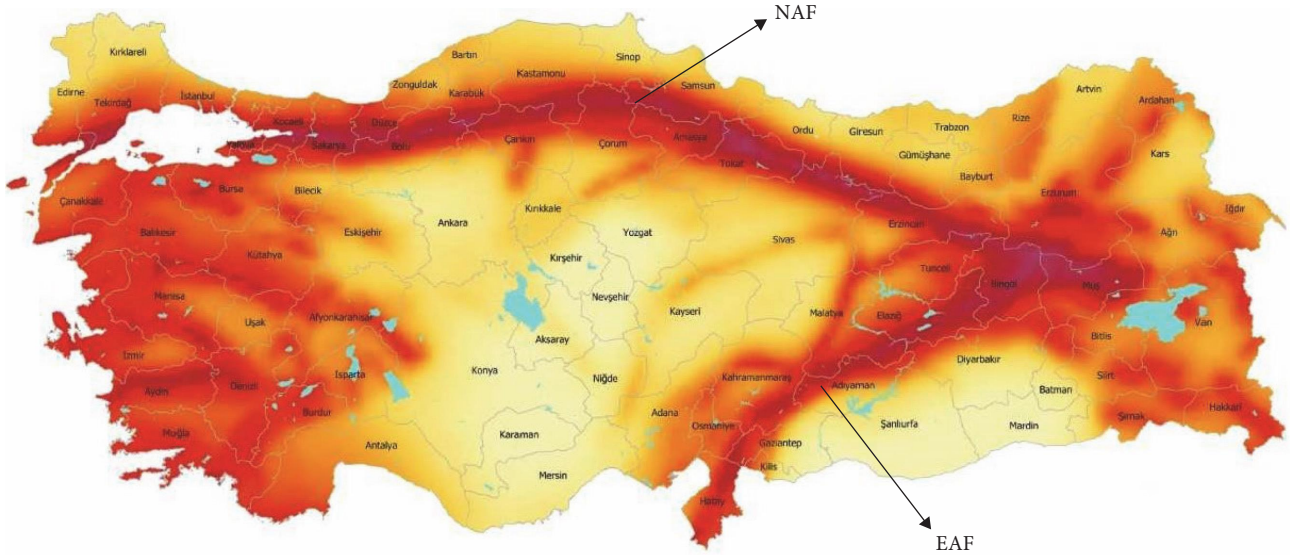

Figure 2: Seismic hazard map of Turkey [29, 30].

intervals. This earthquake occurred close to the Ermenek Dam and may have caused significant changes in the earthquake behavior of the Ermenek Dam. For this reason, it is vital to examine the earthquake behavior of the Ermenek Dam, taking into account the 2023 earthquakes in Turkey.

4. Seismic Properties of the Zone where Constructed Ermenek Arch Dam

Turkey is a country caught between important earthquake fault lines. Many severe earthquakes have occurred in Turkey from the past to the present. For this reason, it is of great importance to examine the seismicity of important water structures such as dams in Turkey. The seismic hazard map of Turkey is shown in Figure 2 [30]. North Anatolian Fault and EAF are the main fault lines producing strong earthquakes. EAF is one of the most important faults that has 30 km width and 580 km length. This fault system comprises the region between Kargapazarı and the west of Çelikhan. EAF fault line bifurcates at this location, and the south branch of the fault starts from the north of Pazarcık (the location of the recent earthquake) and ends up in the Türkoğlu junction, while the north branch of the fault contains the Osmaniye-Karataş fault [30].

EAF has a long seismic ground motion history. Palu, in 1789, is the first known earthquake in EAFS. Six significant earthquakes (1822, 1866, 1872, 1874, 1875, and 1893) occurred in the 19th century. The frequency of the earthquake got slowdown in the 20th century. Three earthquakes happened in this century, and only one of them (Bingöl earthquake Ms = 6.8) seems to be strong. In this fault zone, earthquakes become more often in the 21st century compared to other centuries. Earthquakes generated in this region for this century were 2003 Bingöl (Mw 6.3), 2005 Karlıova Bingöl (Mw 5.8), 2007 Doğanyol Malatya (Mw 5.7), 2010 Kovancılar Elazığ (Mw 6.1), 2020 Sivirice Elazığ (Mw 5.8), and 2020 Karlıova Bingöl (Mw 5.7). Recent earthquakes that occurred in EAFS are Pazarcık Kahramanmaraş (Mw 7.7), Nurdağı Gaziantep (Mw 6.6), Elbistan Kahramanmaraş (Mw 7.6), and Yayladağı Hatay (Mw 6.4). The first three earthquakes happened on the same day (February 6, 2023). The Gaziantep earthquake occurred only 11 min after the Pazarcık earthquake. Distance from the epicenter of the earthquake was very close to Kahramanmaraş (31.26 km). Elbistan earthquake hit the same city (Kahramanmaraş) just 9 hr after the Pazarcık earthquake [30]. The last earthquake (Hatay) that finished the series occurred only after 14 days (February 20, 2023). These earthquakes caused significant damage to the structures. The appearance and location of the earthquakes that occurred in Turkey in 2023 are shown in detail in Figure 3.

5. 3D Finite-Difference Modeling of Ermenek Dam

It is of great importance to evaluate the 3D behavior of the Ermenek Dam and to examine the seismic finite-difference behavior of the dam under the severe earthquakes that occurred in the provinces of Kahramanmaraş, Hatay, Gaziantep, and Malatya in 2023. In this study, the finite-difference method-based WD material model is used for the concrete material of the dam. This material model literature provides new insights into the seismic plastic damage behavior of arch dams. While creating the dam's finite-difference model, the gallery spaces of the dam are first modeled. Moreover, the cylindrical block command line in the FLAC3D program is used when creating the gallery spaces of the dam. The upper part of the gallery is cylindrical, while the lower part is rectangular. While creating four different gallery spaces in the dam body, attention is paid to modeling the contraction joints used in the dam body separately. There are 10 different contraction joints in the dam body. The foundation part is extended towards the upstream part by three times the dam body length [31, 32]. In addition, the foundation is extended downstream and upstream as the dam body. After the body-foundation system of the dam is modeled,

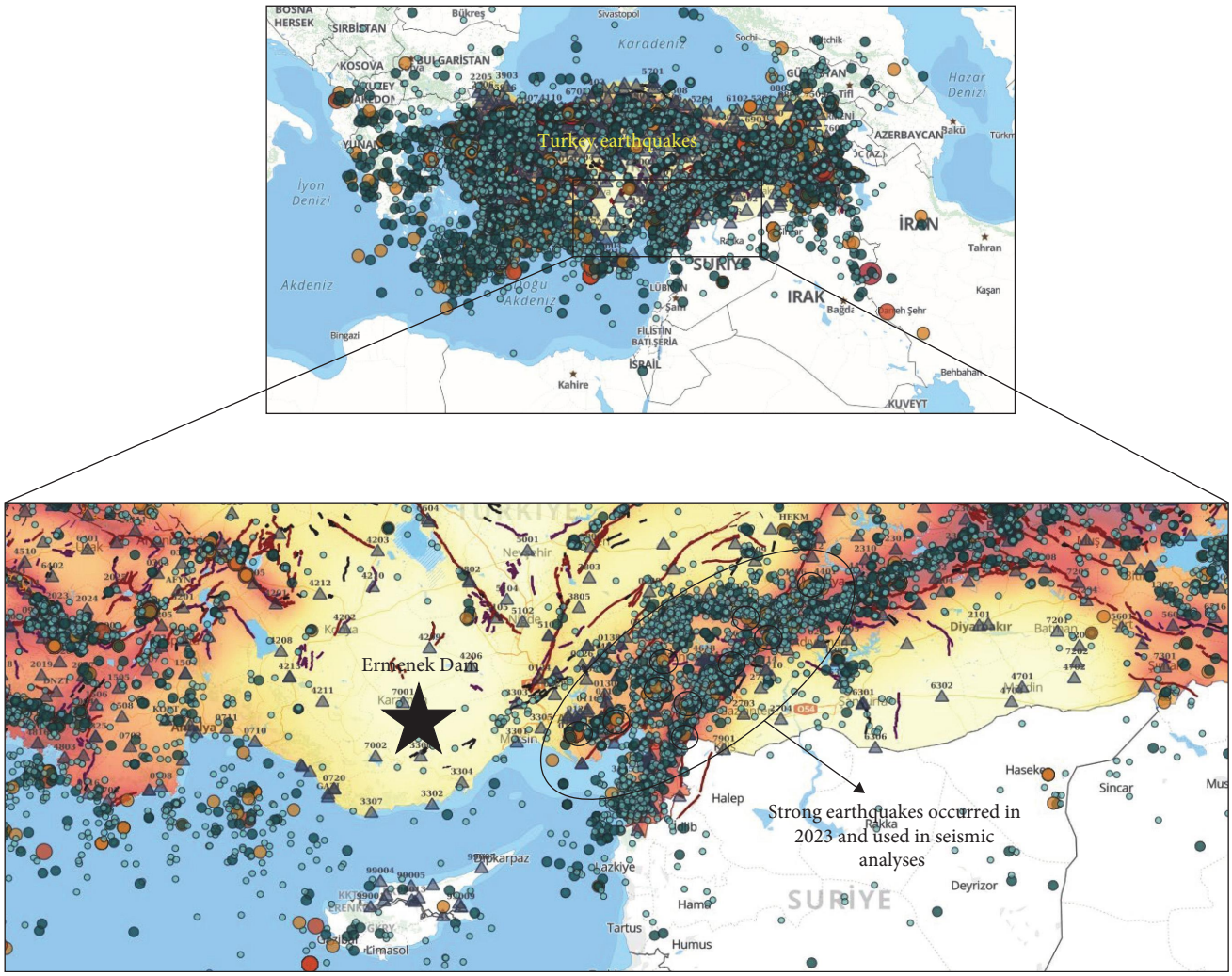

Figure 3: View of earthquakes that occurred on the EAF in 2023 [30].

fix reflecting boundary condition is defined on the lateral boundaries of the dam. Only fix reflecting boundary elements in the z direction are defined at the base of the foundation. Also, quiet nonreflecting, and free-field boundary elements are identified for the foundation lateral boundaries. Hysteresis damping is calculated separately for the dam concrete material and the foundation, and the calculated damping is included in the seismic analysis with the help of fish functions. Separate dynamic time intervals are defined for each seismic analysis. For the concrete material of the dam, bulk modulus, material parameter, WIPP model constant (A, B, D), WIPP model exponent, Poisson's ratio, shear modulus, and tension limit are defined in the program with the aid of fish functions. Thanks to this material model, the seismic plastic damage of the dam concrete is modeled realistically. A two-dimensional view of the dam is shown in Figure 4.

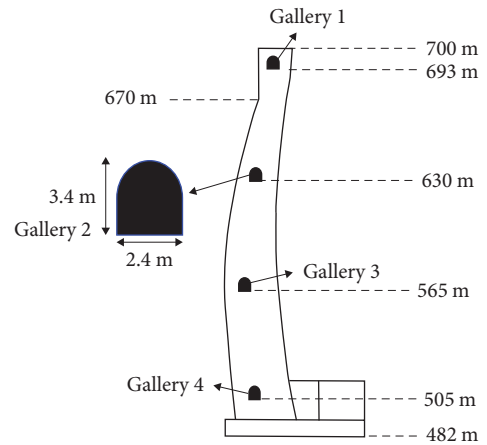

Figure 4: Two-dimensional view of the dam.

Contraction joints play a significant role in the design and construction of arch dams. They are specifically incorporated to accommodate the anticipated volume changes resulting from temperature fluctuations and material shrinkage. Contraction joints help to mitigate the development of excessive tensile stresses, which can lead to cracking and potential structural instability in the dam. Contraction joints are essentially deliberate gaps or discontinuities introduced at predetermined locations within the arch dam. These joints allow for controlled movement and provide a release mechanism for

stress-induced deformations. The design of contraction joints takes into account factors such as the dam's geometry, material properties, and expected thermal and shrinkage effects. In terms of modeling contraction joints, FLAC3D, and similar software packages offer various techniques to simulate their behavior. One commonly used approach is to incorporate discrete joint elements within the numerical model. These joint elements have specific properties that allow for controlled separation and sliding along the joint surfaces. To model contraction joints in FLAC3D, we followed these general steps:

(i) Geometry definition: Define the geometry of the contraction joints within the arch dam model. This involves specifying the locations, orientations, and dimensions of the joints. Contraction joints are typically vertical or inclined planes that intersect the dam structure.

(ii) Joint element creation: Create joint elements along the defined joint planes. These elements act as interfaces that can separate and slide, allowing for movement and deformation across the joint surfaces. Assign appropriate properties to the joint elements, such as friction coefficients and shear strength parameters, to represent the behavior of the actual joints.

(iii) Joint behavior and interaction: Define the behavior of the joint elements in response to loading and displacement conditions. This includes specifying the allowed separation, sliding, and rotation along the joint surfaces. Consider the joint properties, such as joint stiffness, strength, and dilation, to accurately represent the anticipated behavior of contraction joints.

(iv) Analysis and interpretation: Conduct the numerical analysis using FLAC3D, considering the defined contraction joints. Monitor and analyze the deformation and stress distribution across the joints to assess the performance and integrity of the arch dam under various loading conditions.

In this study, the contraction joints in the finite-difference model of the Ermenek Arch Dam, which is modeled in three dimensions, are shown in detail in Figure 5. A water table is created to model the reservoir water in the upstream part of the dam. Besides, hydrostatic forces are applied to each mesh edge in the upstream part depending on the height. To determine the seismic behavior of the Ermenek Dam, the earthquakes that occurred in Kahramanmaraş, Malatya, Hatay, and Gaziantep provinces of Turkey in 2023, which caused the death of thousands of people, are utilized. The 3D finite-difference model of the Ermenek Arch Dam is shown in Figure 5. Moreover, the mechanical properties of earthquakes used in seismic analyses are shown in Table 1 in detail. The primary objective of this research is to investigate the response of arch dams to a diverse set of seismic events. By incorporating earthquakes with varying PGA into numerical analyses, it was aimed to capture a wide range of ground motion characteristics. The earthquakes selected for examining the seismic behavior of the Ermenek Dam are of significant importance, as they represent notable seismic events that occurred in Turkey in 2023. In the study, these earthquakes were listed based on their chronological occurrence. Although the order of the earthquakes may appear mixed, it was necessary to prioritize them in this manner, as the sequence of earthquakes plays a vital role in determining the dam's seismic behavior. It is important to note that the primary focus of this study is not to explore the specific characteristics of individual earthquakes and their effects on the dam's behavior. Rather, the main objective of this study is to analyze the impacts of the 2023 earthquakes in Kahramanmaraş, Gaziantep, Malatya, and Hatay on the structural response of the Ermenek Dam. For this reason, earthquakes were listed in chronological order, and analyses were made according to this order.

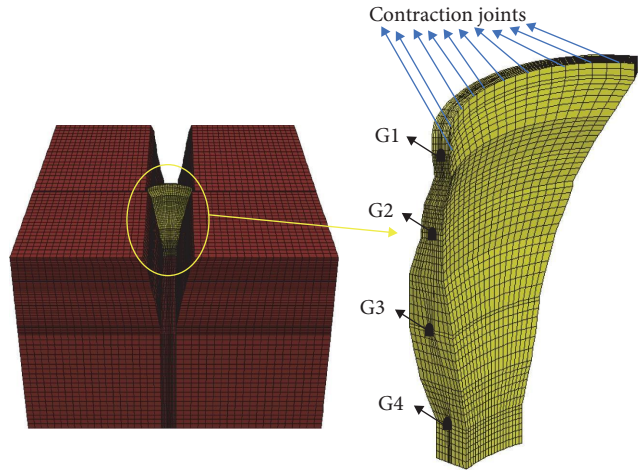

Figure 5: Three-dimensional finite-difference model of Ermenek Arch Dam.

The Kahramanmaraş earthquakes (Mw 7.7 and Mw 7.6) emerge as the most severe seismic events, resulting in the most substantial seismic effects on the dam. These earthquakes have been highlighted as they pose the greatest potential risk to the structural integrity of the arch dam.

6. Results and Discussion

Examining the seismic crack and failure response of essential buildings such as arch dams is noteworthy for their sustainability. In this section, the earthquake failure behavior of the Ermenek Arch Dam is examined by considering 10 different strong ground motions (Table 1). After the seismic accelerations are identified in the FLAC3D software with the help of fish functions, seismic accelerations are affected by the foundation. Moreover, seismic accelerations are defined in the program by considering the X, Y, and Z directions of the earthquakes. The analysis chart for seismic failure analyses is shown in Figure 6.

The FLAC3D software made many errors while performing the seismic analyses of the dam, and therefore the mesh

Table 1: Earthquake characteristics [30].

Case	Earthquake	Mw	Distance (km)	PGA (cm^2/s)	PGV (cm/s)	PGD (s)
1	Pazarcık (Kahramanmaraş)	5.5	6.87	49.84	2.84	0.55
2	İslahiye (Gaziantep)	5.7	10.46	363.52	13.85	1.02
3	Ekinözü (Kahramanmaraş)	5.5	10.93	79.35	4.26	0.42
4	Pazarcık (Kahramanmaraş)	7.6	8.6	1,966.74	186.78	661.9
5	Elbistan (Kahramanmaraş)	7.6	7	635.45	170.79	614.52
6	Yeşilyurt (Malatya)	5.6	6.15	25.23	2.36	12.77
7	Nurdağı (Gaziantep)	6.6	6.2	445.29	40.49	9.27
8	Doğanşehir (Malatya)	5.6	10.23	47.28	2.90	0.40
9	Nurdağı (Gaziantep)	5.6	6.98	44.15	2.91	0.73
10	Defne (Hatay)	6.4	21.7	445.38	75.78	44.90

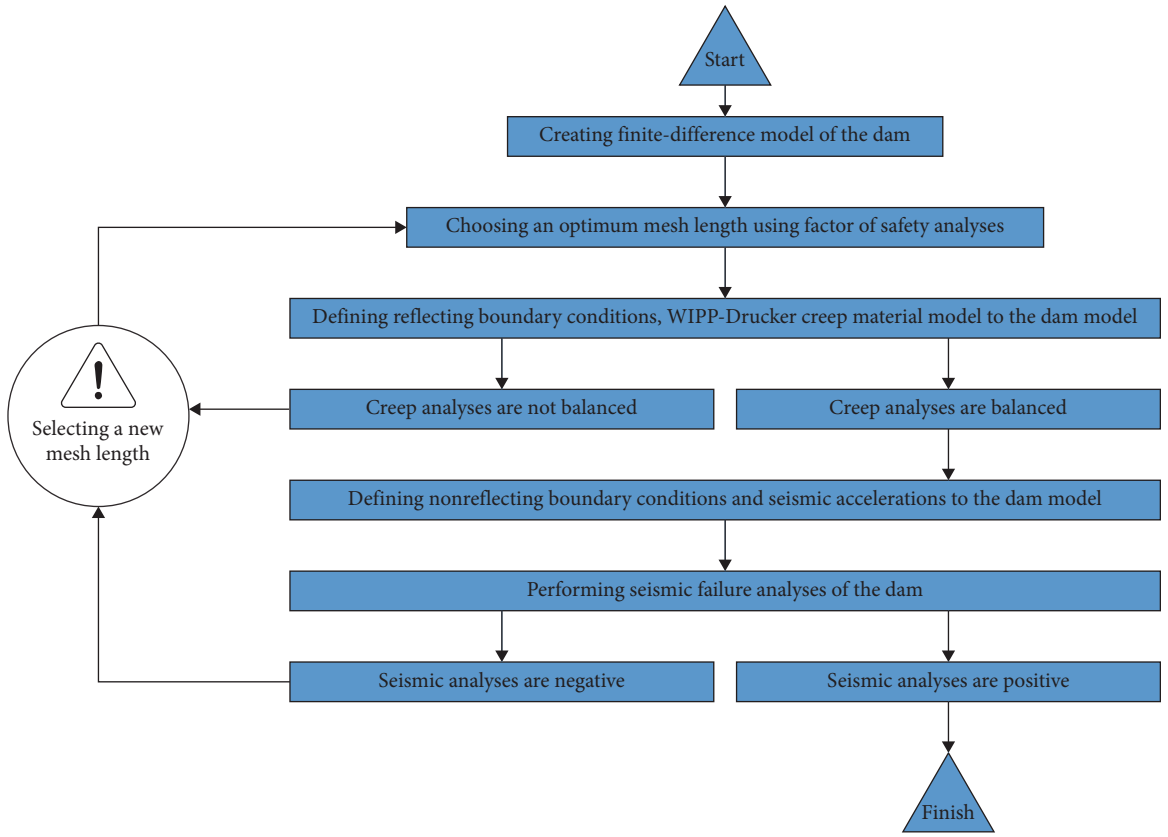

Figure 6: Analysis chart of seismic analyses.

lengths of the dam model were changed many times. Because the propagation of each seismic wave in the model is different, and different mesh intervals are determined for each seismic analysis. To find the optimum mesh range of the Ermenek Dam, the FOS analyses were performed for different mesh ranges. The primary purpose of FOS analyses performed in the FLAC3D program is to assess the stability and safety of geotechnical structures or systems. The FOS is a ratio that compares the capacity of a structure or material to resist applied loads to the actual loads exerted on it. It serves as an indicator of the stability and reliability of the analyzed system. By conducting FOS analyses in FLAC3D, engineers and researchers can evaluate the potential for failure or instability in geotechnical structures such as slopes, tunnels, foundations, and retaining walls. The analysis involves considering various factors, including the properties of the materials involved, the geometry of the structure, and the applied loads or boundary conditions. The FOS is typically calculated by comparing the shear strength of the soil or rock material to the forces acting upon it. If the FOS is less than 1, it indicates that the structure or system is prone to failure, as the applied loads exceed the capacity of the material to resist them. On the other hand, a FOS greater than 1 indicates a higher level of stability, providing a margin of safety against potential failure. In FLAC3D, FOS analyses allow engineers to make informed decisions in design, construction, and risk assessment

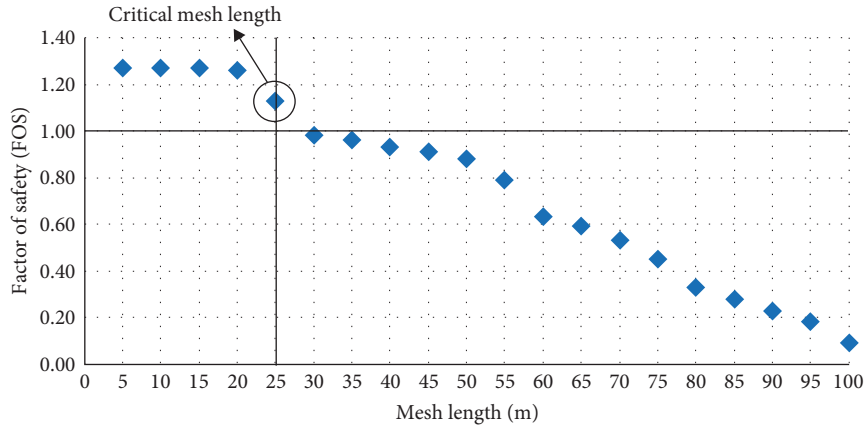

Figure 7: Optimum mesh space for Ermenek Arch Dam.

processes. By examining different scenarios, modifying input parameters, and considering uncertainties, engineers can optimize designs, identify potential failure mechanisms, and implement appropriate mitigation measures to ensure the safety and stability of geotechnical structures. Overall, the FOS analyses in the FLAC3D program play a crucial role in evaluating the stability and reliability of geotechnical systems, enabling engineers to make informed decisions and enhance the safety of various construction projects. For this reason, FOS analyses were carried out in this study, and different dimensions of the brick elements used in the 3D finite-difference model of the dam were taken into account while performing the analyses. The term "mesh space" used in the study represents the size of each brick element. In addition, random mesh space (mesh width) is used for seismic analysis of arch dams in the literature. However, each mesh space creates different seismic effects on the seismic behavior of the dam. For this reason, in this study, it is aimed to eliminate this confusion and uncertainty in the literature, and the most suitable mesh space is used for the seismic behavior of the Ermenek Arch Dam. The FOS analyses are used in the FLAC3D program with the help of special fish functions and are based on the strength reduction method [26]. This method is applied to reveal the safety factors of all underground and aboveground special structures. Furthermore, although this method is generally used with the Mohr–Coulomb material model, it is also compatible with other material models in FLAC3D [26]. The "strength reduction technique" is practiced in FOS calculations by progressively reducing the shear strength of the material to bring the slope to a state of limiting equilibrium [26]. The safety factor (F) is defined according to the equations:

$$c^{\text{trial}} = \frac{c}{F^{\text{trial}}}. \tag{19}$$

$$\phi^{\text{trial}} = \arctan\left(\frac{\tan\phi}{F^{\text{trial}}}\right). \tag{20}$$

A series of simulations are performed utilizing trial values of the factor F^{trial} to reduce the cohesion and friction angle until slope failure occurs [26]. If the slope is initially unstable, it will be increased until the limiting condition is found [26]. The FOS analyses are performed for 20 different mesh ranges of the dam (Figure 7). According to the FOS analyses, it is observed that the FOS value of the dam is below 1 if the mesh space of the dam is between 30 and 100 m. However, for the dam to be safe, the FOS values must be above 1. Then, it is concluded that the FOS values are above 1 if the mesh space of the dam is 25, 20, 15, 10, and 5 m. For this reason, attention is paid to ensuring that the mesh space of the dam is between 5 and 25 m for seismic analyses (Figure 7). From this result, it is suggested that random mesh ranges should not be chosen for seismic analysis of arch dams. Obtaining the initial natural frequencies of a structure is crucial when studying its dynamic response. In this case, the dynamic behavior of the Ermenek arch dam is investigated, considering the influence of water on the natural frequencies. The finite difference model of this high arch dam reveals the first six natural frequencies as follows: 1.18, 1.26, 1.89, 1.97, 2.06, and 2.18 Hz. In addition, earthquakes are listed in Table 1 according to their intensity, and Kahramanmaraş earthquakes (Mw 7.7 and Mw 7.6), which are the most severe earthquakes, have created the most serious seismic effects on the dam. Figures 8–17 show the principal stress results that occurred along with the dam height for 10 different seismic analyses. Analysis results for empty and full water conditions of the dam are shown in the graphs. The empty water condition of the dam is called Situation 1, and the full water condition of the dam is called Situation 2. In Figure 8, the seismic analysis results are presented for the Case 1 earthquake in detail. According to Figure 8, it is seen that there are very large seismic stress differences between Situation 1 and Situation 2 of the dam. This result clearly shows the reservoir water height effects on the seismic response of arch dams. Besides, it is observed that very large principal stresses occurred in the locations close to the gallery spaces of arch dams during the Case 1 earthquake. The largest principal stress values for the dam's Situation 2 occurred around G2. Moreover, for Situation 2, it is understood that the greatest principal stress values took place around G3. It is concluded from these results that gallery spaces have a great effect

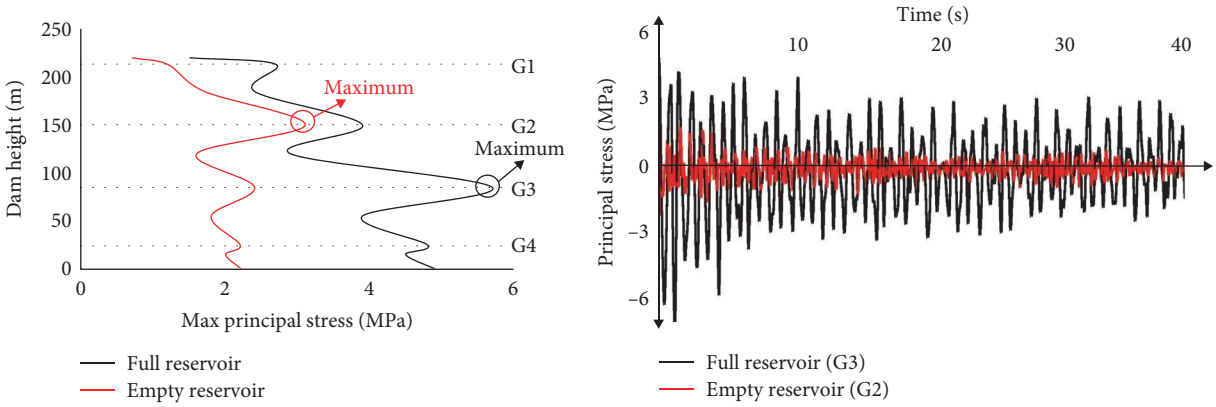

Figure 8: Seismic principal stress results of the dam for Case 1.

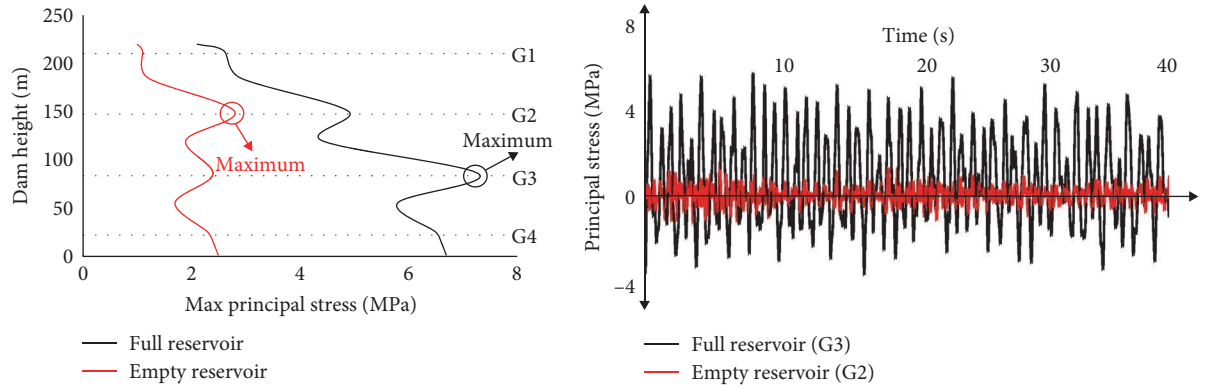

Figure 9: Seismic principal stress results of the dam for Case 2.

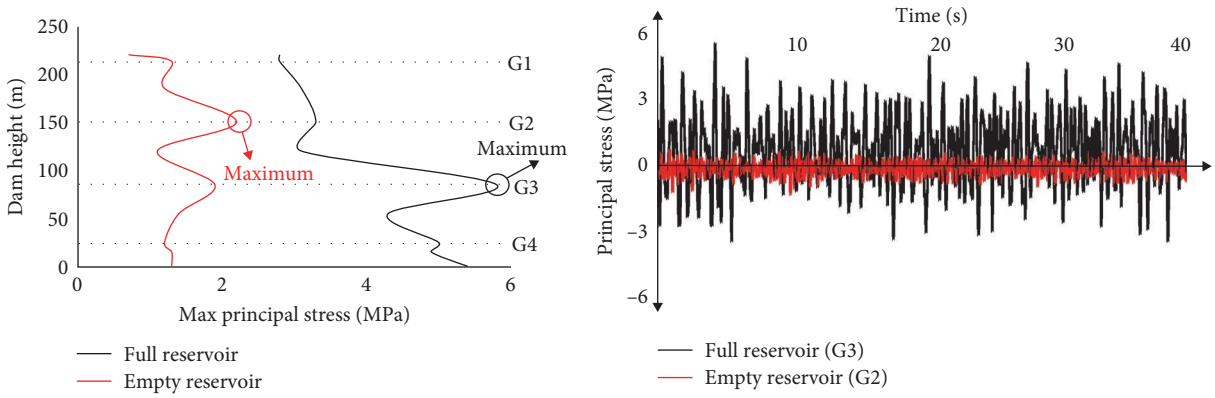

Figure 10: Seismic principal stress results of the dam for Case 3.

on the seismic response of arch dams. For Situation 1 and Situation 2 of the dam, the smallest principal stress values happened around G1 (Figure 8).

In Figure 9, the seismic failure response of the Ermenek Dam is assessed for Case 2. According to Figure 9, the largest principal stress values for Situation 2 are observed around G2. Furthermore, the largest principal values for Situation 2 took place around G3. It is observed that G3 is the most important section of the arch dams for the seismic safety of the dam. For the empty water situation of the arch dam, the greatest stress, value occurring during the Case 2 earthquake is 7.49 MPa while it is only 2.82 MPa for the full reservoir. In Figure 10, the seismic response of the Ermenek Dam is examined for the Case 3 earthquake. According to Figure 10, the greatest principal stress values for Situation 2 are observed around G2. In addition, the smallest principal stress values along the dam height are observed around G1. According to Situation 2 of the dam, it is observed that the

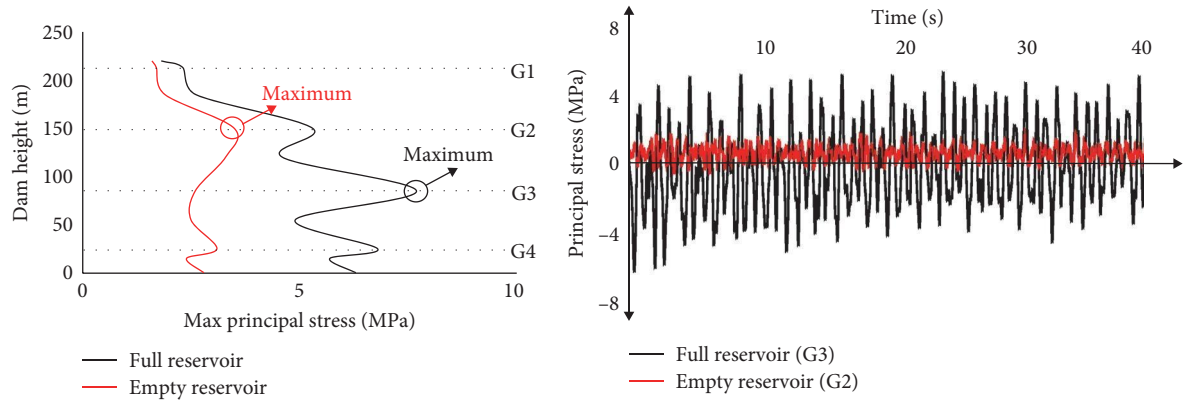

Figure 11: Seismic principal stress results of the dam for Case 4.

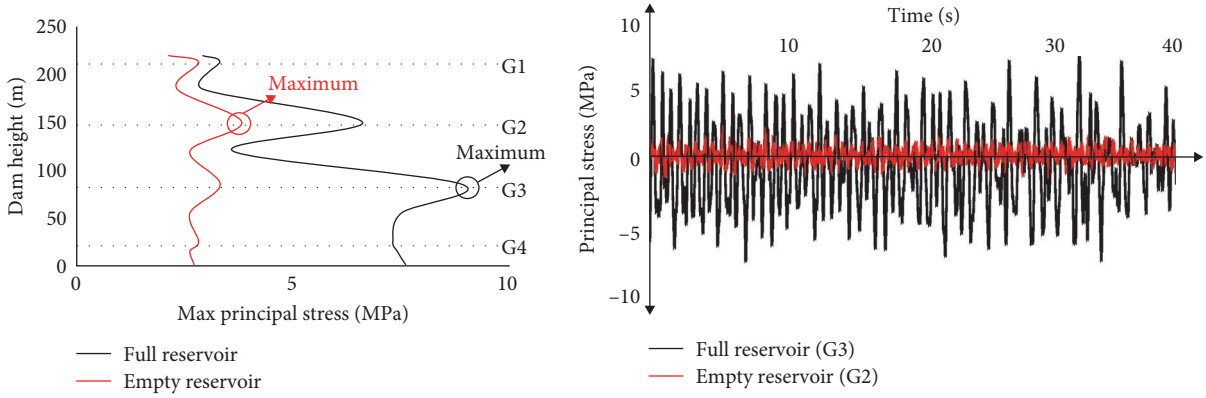

Figure 12: Seismic principal stress results of the dam for Case 5.

biggest principal stresses in the body took place on G3. It is understood from these results that the most critical sections for the earthquake failure behavior of arch dams are G3 and G2, respectively. Moreover, the reservoir height effects on the earthquake failure behavior of arch dams are revealed from these results.

In Figure 11, the seismic failure response of the Ermenek Dam is examined for the Case 4 earthquake. According to Figure 11, the smallest principal stress values for Situation 2 are observed around G2. Furthermore, the largest principal stress values that took place in the dam body for Situation 2 are obtained around G2. However, larger principal stress values are obtained in the dam body for Situation 2 of the dam. The greatest principal stress values occurred around G3 along with the dam height, and the greatest principal stress value (8.1 MPa) happened around G3. For Situation 2 of the dam, the peak principal stress values around G3 and G4 are very close to each other. In Figure 12, the Ermenek Dam's seismic response is assessed for the Case 5 earthquake. It is seen that the seismic failure response of the dam for the Case 4 earthquake and Case 5 earthquake is very similar to each other, and the smallest principal stress values for the empty reservoir situation occurred around G4. Besides, the largest principal stress values acquired along the dam height are observed around G3. For Situation 2 of the dam, the biggest principal stress values in the dam body are gained around G3. Also, the greatest principal stress values around G3 and G4 for Situation 2 are 9.2 and 7.2 MPa, respectively. The effects of gallery spaces on the seismic failure behavior of high arch dams are understood from these results.

In Figure 13, the seismic response of the Ermenek Dam is examined for the Case 6 earthquake in detail, and very important seismic failure differences are observed for Situation 1 and Situation 2 of the dam. The largest principal stress value for Situation 2 is 3.92 MPa, and this numerical value took place around G2. In addition, for Situation 2 of the dam, the largest principal stress value along the dam height is observed around G3. Close seismic principal stress values are acquired around the G3 and G4. As the time-history analysis results for G3 are examined, it is clear that the greatest principal stress value around the gallery occurred in the 38th second of the earthquake. In Figure 14, the seismic failure response of the Ermenek Dam is examined for the Case 7 earthquake. According to Figure 14, the smallest principal stress values for the empty reservoir situation are observed around G1. Besides, the largest principal stress values are obtained around G2. Principal stress values around G3 and G4 are close to each other. For Situation 2 of the dam, the largest principal stress value is 9.3 MPa, and this numerical value is observed around G3. Furthermore, the largest principal stress value around G3 occurred in the 2nd second of the earthquake. From this result, it is clearly understood that gallery spaces are very critical for the seismic response of high arch dams.

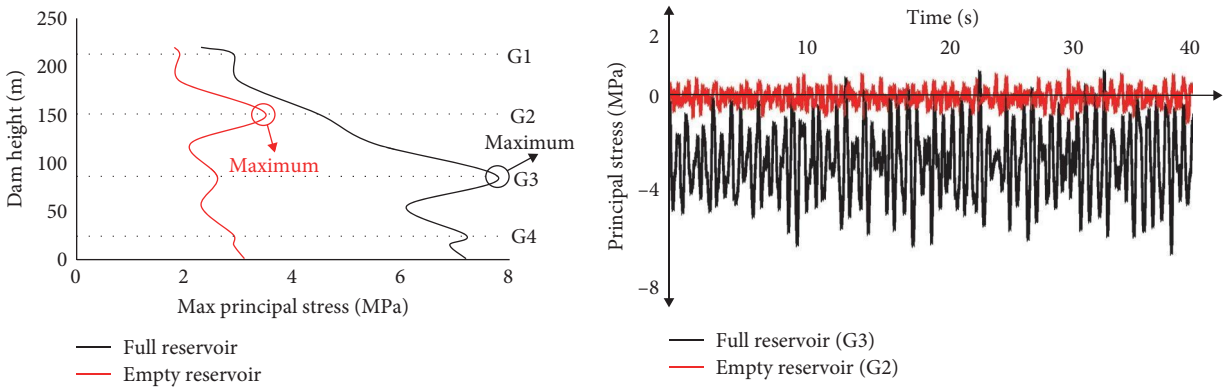

Figure 13: Seismic principal stress results of the dam for Case 6.

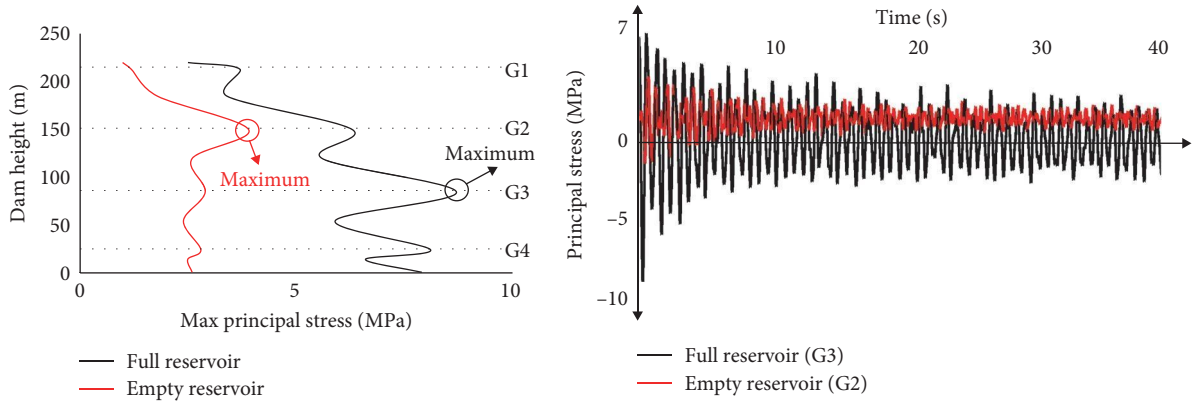

Figure 14: Seismic principal stress results of the dam for Case 7.

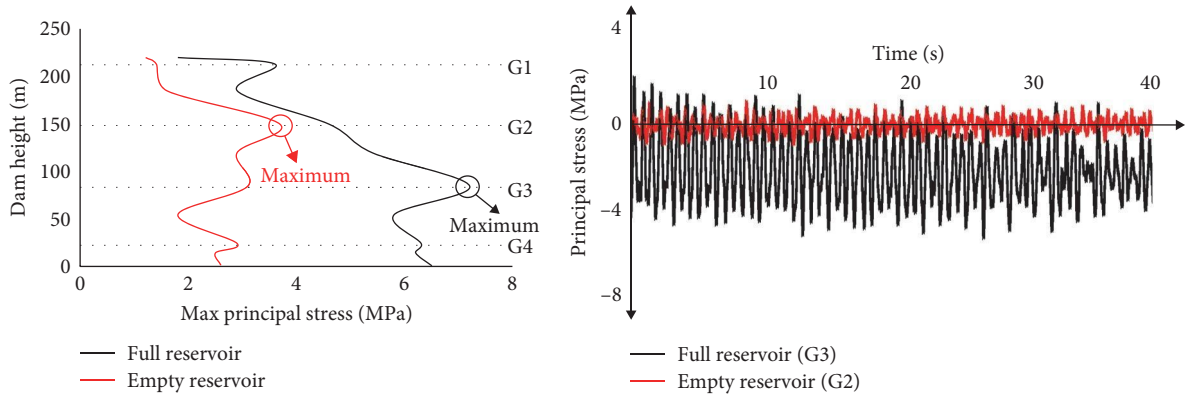

Figure 15: Seismic principal stress results of the dam for Case 8.

In Figure 15, the seismic response of the Ermenek Dam is observed for Case 8. The largest stresses for the empty water situation are acquired around G2. Besides, close seismic principal stress values are observed around G3 and G4. For Situation 2, the largest principal stress values took place along the dam body around G3. Smaller principal stress values are observed in G2 when compared to G4. The importance of both reservoir height and gallery spaces for the earthquake behavior of arch dams is understood from these results. In Figure 16, the response to the seismic failure of the Ermenek Dam is evaluated for Case 9. According to Figure 16, it is understood that the seismic principal stress values obtained for Situation 2 are more critical than Situation 1. Besides, the largest principal stress value for Situation 2 of the dam is 7.2 MPa, and this numerical value is obtained around G3. In Figure 17, the seismic response of the dam is examined for Case 10. When the dam is examined in an empty reservoir situation, it is clearly understood that for Case 10, the largest principal stress values in the dam body are obtained around G3. Moreover, close principal stress values are observed for G2 and G4. The largest principal stress value for

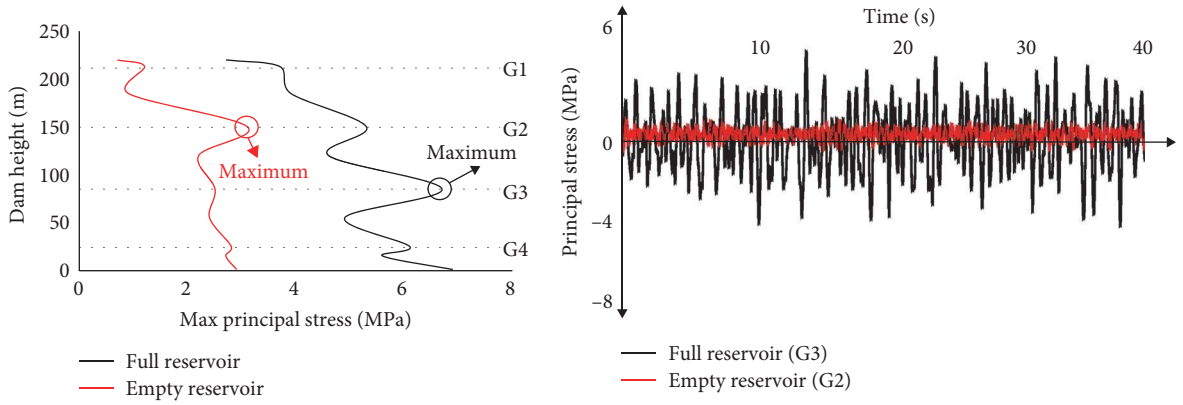

Figure 16: Seismic principal stress results of the dam for Case 9.

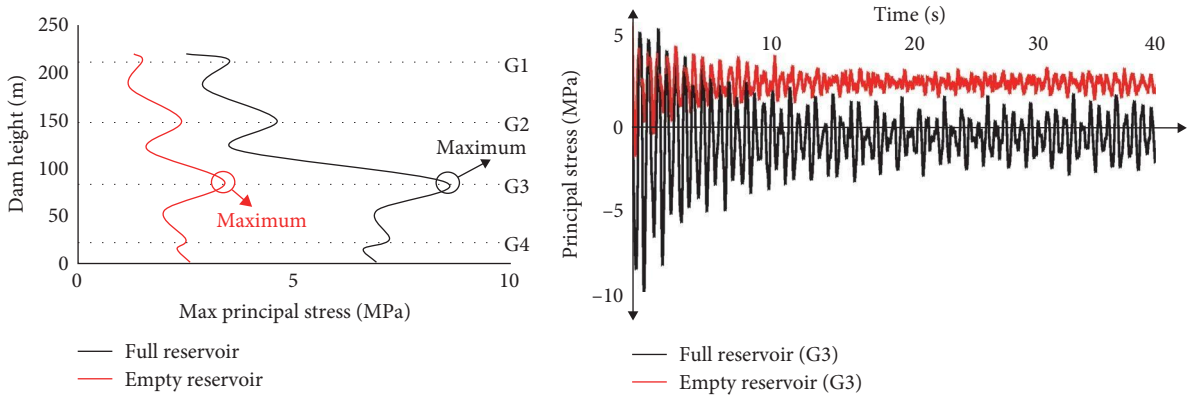

Figure 17: Seismic principal stress results of the dam for Case 10.

Situation 2 of the dam is 8.4 MPa, and this numerical value is gained around G3. From these results, it is recommended to include gallery spaces in the modeling and analysis of the arch dams. Furthermore, it is concluded that gallery spaces' effect on the earthquake behavior of arch dams is significant.

In Figures 18–27, the seismic crack response of the Ermenek Dam is examined under 10 different strong ground motions. Special fish functions were written in the FLAC3D program to obtain cracks. To obtain cracks in a modeled arch dam using the FLAC3D program, it was followed a procedure that involves incorporating appropriate material properties and defining suitable modeling techniques. Here is a step-by-step explanation:

(i) Assign appropriate material properties to the dam material, considering its behavior under tensile stress. It is crucial to define a material model that can capture the initiation and propagation of cracks. Commonly used material models for concrete dams include the Mohr–Coulomb or Hoek–Brown models, which incorporate fracture parameters.

(ii) Select elements in the FLAC3D model where cracks are expected to occur. This can be done by identifying regions of potential tensile stress concentrations, such as areas with high bending moments or areas near supports. Ensure that the selected elements have proper mesh refinement to capture localized crack development accurately.

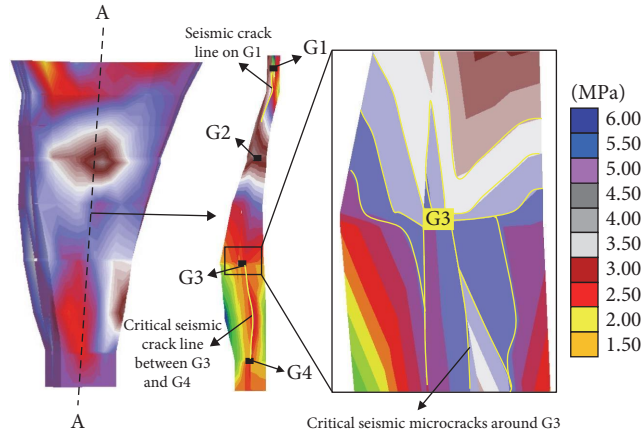

Figure 18: Seismic crack results of the dam for Case 1.

(iii) Specify the initial cracks within the selected elements. You can define cracks by inserting them manually at desired locations or by using automated techniques available in FLAC3D, such as crack propagation algorithms or predefined crack patterns.

(iv) Define the criteria for crack propagation within the model. This can be based on stress thresholds, strain

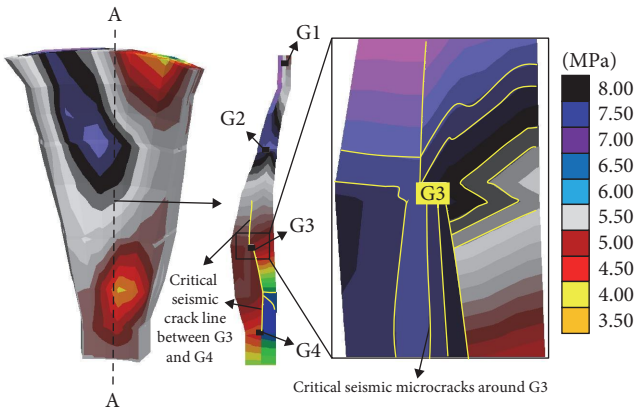

Figure 19: Seismic crack results of the dam for Case 2.

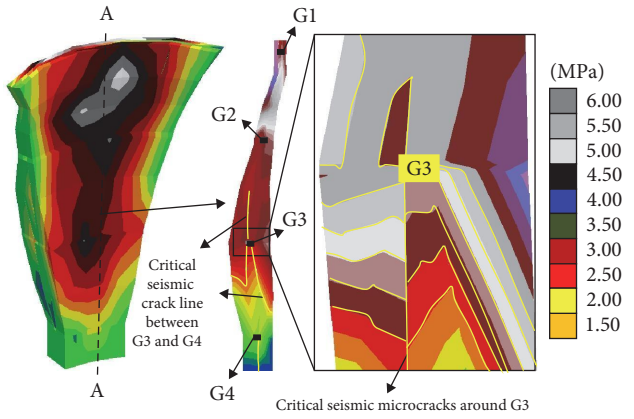

Figure 20: Seismic crack results of the dam for Case 3.

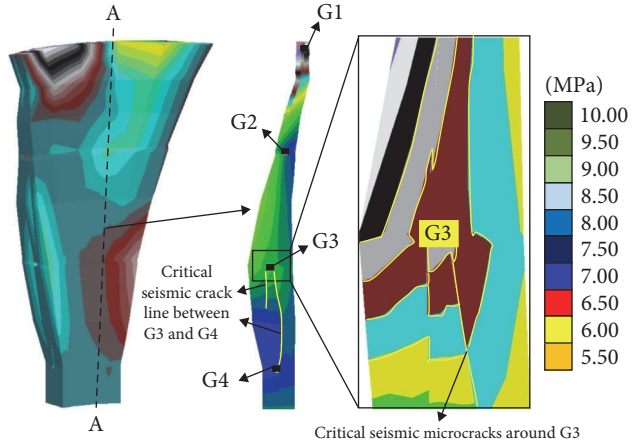

Figure 21: Seismic crack results of the dam for Case 4.

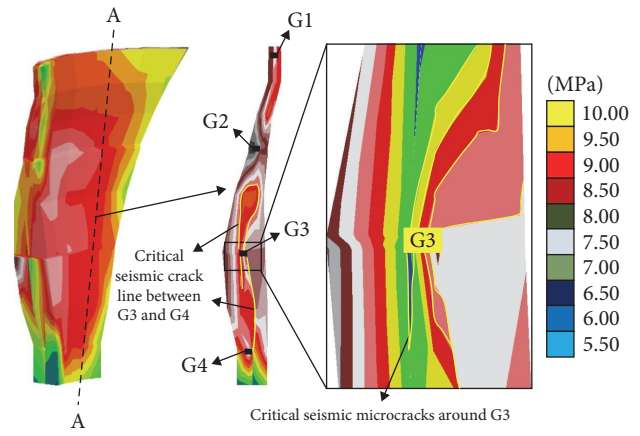

Figure 22: Seismic crack results of the dam for Case 5.

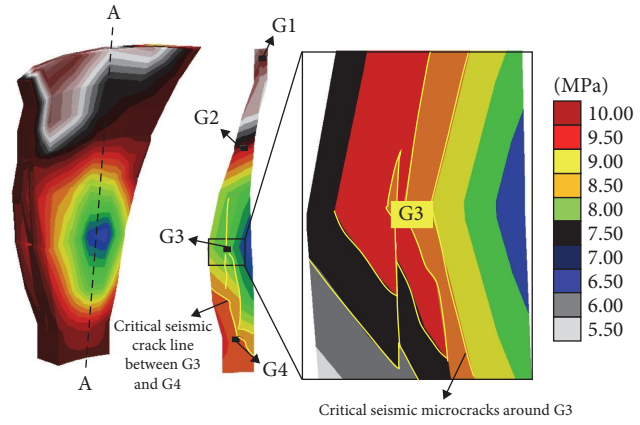

Figure 23: Seismic crack results of the dam for Case 6.

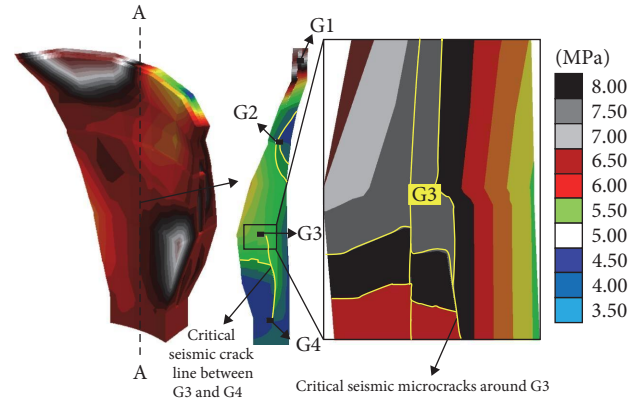

Figure 24: Seismic crack results of the dam for Case 7.

energy release rates, or other fracture mechanics parameters. As the analysis progresses, the model will simulate the growth and extension of cracks according to the defined criteria.

(v) Utilize postprocessing tools in FLAC3D to visualize the cracks in the dam model. This can include generating contour plots of crack orientations, lengths, or opening displacements. Additionally, you can display crack profiles or generate 3D renderings to better understand the distribution and evolution of cracks within the arch dam.

It is seen from seismic analyses that critical cracks occurred around the gallery spaces in the dam body during the earthquake. These cracks may adversely affect the structural response of the dam. For this reason, it is suggested that

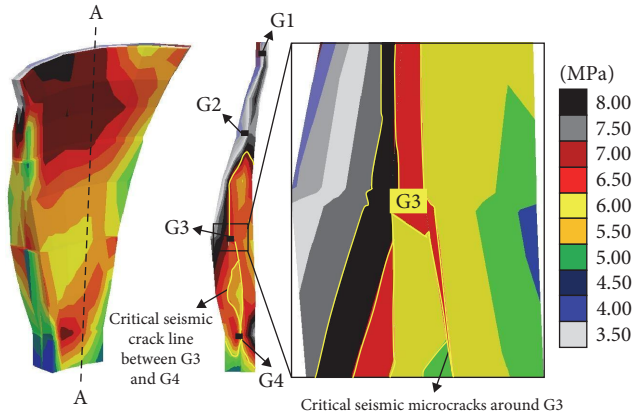

Figure 25: Seismic crack results of the dam for Case 8.

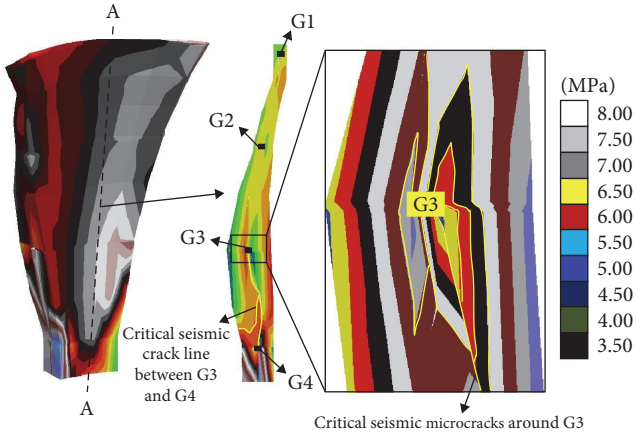

Figure 26: Seismic crack results of the dam for Case 9.

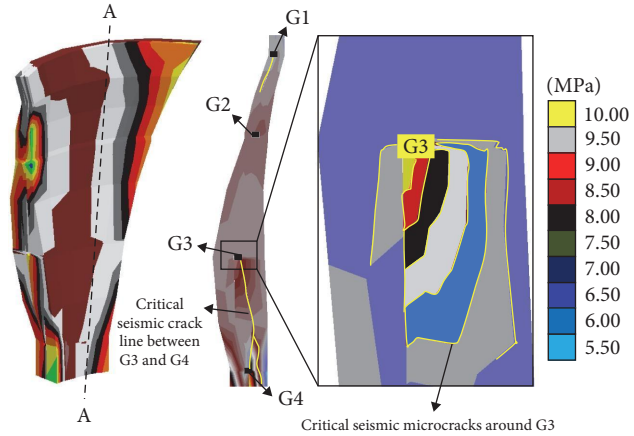

Figure 27: Seismic crack results of the dam for Case 10.

the gallery spaces should be carefully modeled and constructed, taking into account the seismicity of the area where the dam is located. In Figure 18, the seismic crack response of the Ermenek Dam is examined for Case 1. For Case 1, it is observed that the most serious cracks occurred between G3 and G4 during the earthquake. From this result, it is understood that G3 and G4 are the most critical sections for the seismic crack response of arch dams. It is also concluded that critical cracks took place in the lower sides of G1 during the earthquake. When the seismic cracks around G3 are assessed, it is clearly understood that microcracks can occur up and down sections of the gallery spaces. It is also concluded that severe principal stresses occurred in close sections to G3 (Figure 18). In Figure 19, the seismic crack response of the Ermenek Dam is evaluated for Case 2. According to Figure 19, significant cracks are observed around G3. This result clearly shows that G3 is the most critical section for the seismic response of arch dams. Besides, significant cracks are observed between G2 and G3, and it is understood that G3 should be modeled well while modeling and analyzing arch dams (Figure 19).

In Figure 20, the seismic crack response of the Ermenek Dam is examined for Case 3. For Case 3, serious cracks are observed in the dam body. The most critical cracks are obtained between G3 and G4. Moreover, no serious cracks are observed around G1 and G2. Very serious seismic principal stress accumulations occurred around G3, and it is concluded that G3 is more critical than other galleries. It is also suggested that gallery spaces are very important for the seismic response of arch dams, and these spaces should be examined separately while checking the arch dam's earthquake safety. In Figure 21, the seismic crack response of the Ermenek Dam is assessed for Case 4. For Case 4, significant seismic cracks are observed between G3 and G4. Serious principal stress values occurred around up and down sections of G3, and these principal stress values also caused serious cracks around G3. Furthermore, significant principal stress values took place around G4. The principal stress values around G3 and G4 are higher than G1 and G2. This result shows the effects of water pressure and gallery spaces on the seismic crack response of arch dams (Figure 21). In Figure 22, the earthquake crack behavior of the Ermenek Dam is assessed for Case 5. When Case 4 and Case 5 are compared with each other, it is openly seen that more seismic principal stress values and seismic cracks occurred in the Ermenek Dam for Case 5. During the earthquake, severe seismic cracks are acquired around G3 and G4, and no significant seismic cracks are observed around G1 and G2. In addition, serious microcracks are obtained between G3 and G4.

In Figure 23, the seismic crack and failure response of the Ermenek Dam is examined for Case 6. For Case 6, very significant seismic cracks are observed around G2 and G3, and serious microcracks occurred between G3 and G4 during the earthquake. These microcracks can significantly change the structural response of the Ermenek Dam. For this reason, it is strongly recommended not to ignore the microcracks that occurred during the earthquake and to pay attention to G3 during the construction and modeling of the arch dams. Moreover, significant seismic principal stress values are acquired around G3. Lower seismic principal stress values are observed around G1 and G2 as compared to G3 and G4. In Figure 24, the earthquake behavior of the arch dam is calculated for Case 7. When comparing Case 6 and Case 7

with each other, larger seismic cracks and seismic principal stresses are observed in the Ermenek Dam body for Case 7. For Case 7, critical seismic cracks took place around G3. Furthermore, it is concluded that G3 is more important for Case 7 than the other gallery. It is observed that the biggest seismic principal stresses in the dam's body occurred around G3 during Case 7. No serious principal stress and seismic cracks are detected around Galleries 1, 2, and 4. Then, it is concluded that G3 is the most critical section for the crack safety of the Ermenek Dam during Case 7.

In Figure 25, the seismic response of the Ermenek Dam is examined for Case 8 in detail. During Case 8, significant seismic cracks occurred in the gallery spaces of the Ermenek Dam body. Very critical seismic cracks are obtained, especially around G3 and G4. Besides, serious cracks took place between G3 and G4. When comparing galleries 1, 2, and 4 with G3, it is concluded that more critical and significant seismic damage occurred around G3 during the earthquake. In Figure 26, the seismic response of the dam is examined for Case 9. The most important seismic cracks that occurred in the dam body during the earthquake are obtained between G3 and G4. Seismic microcracks occurring around G3 may threaten the safety of the dam, and therefore, it is concluded that more attention should be paid to the material parameters used around G3 and the modeling processes of G3. In Figure 27, the seismic principal stress and crack values that took place in the Ermenek Dam body during Case 10 are evaluated in detail. For Case 10, serious seismic principal stresses and cracks occurred around G3 and G4. When 10 different seismic analyses are evaluated, it is concluded that serious cracks may occur around G3 and G4 in arch dams during strong ground motions. However, no significant seismic cracks are observed around G1 and G2 during the earthquake. From these results, the importance of G3 and G4 in arch dams is understood.

In Figures 28–37, the seismic plastic damage states of the Ermenek Arch Dam are investigated under 10 different earthquakes. While obtaining the plastic damage states of the dam, the block state command in the FLAC3D program is used, and after performing seismic analyses in the program, plastic damages in the body of Ermenek Dam are acquired with the help of fish functions. Plastic damage states are shown in shear and tension directions. In addition, the n and p symbols in the contour diagrams represent the damage values of now and past, respectively. Various plastic damage states are detected on the dam body for 10 different earthquakes, and significant plastic damage states occurred on the dam body during the earthquakes. In Figure 28, the earthquake plastic damage state of the Ermenek Dam is evaluated for Case 1. According to Figure 28, no significant damages are acquired in the midsection of the dam body. However, shear (n–p) and tension (n–p) plastic damages are determined at the right and left sides of the dam body. During the Case 1 earthquake, shear (n–p) and tension (p) plastic damage is observed around the gallery spaces in the dam body. From this result, it is understood that the gallery spaces of the arch dams and the right–left sides of their bodies are very important during the earthquake. In Figure 29, the

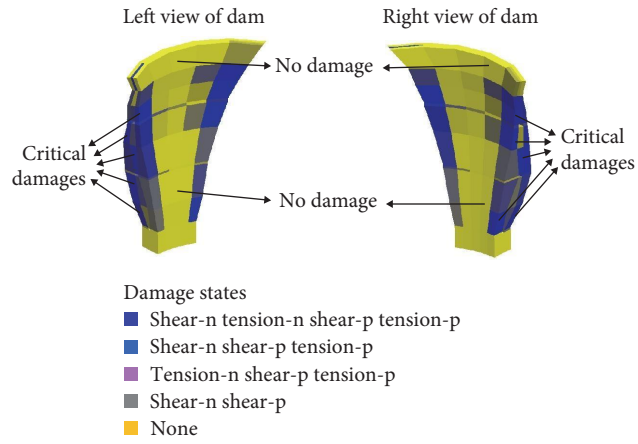

Figure 28: Earthquake damage results of the dam for Case 1.

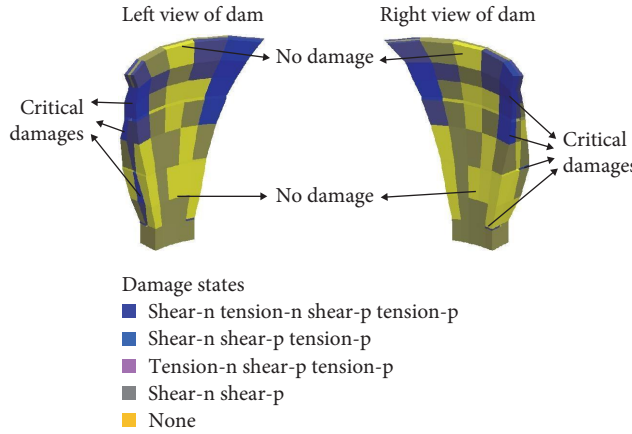

Figure 29: Earthquake damage results of the dam for Case 2.

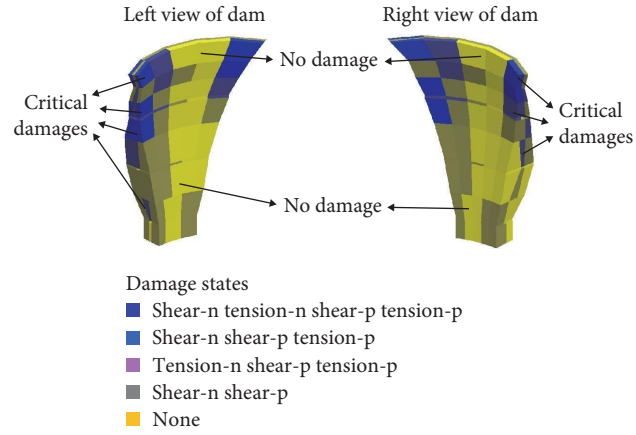

Figure 30: Earthquake damage results of the dam for Case 3.

plastic damage performance of the Ermenek Dam is appraised for Case 2. The plastic damage values taking place in the dam body for Case 2 are similar to Case 1. During the Case 2 earthquake, significant plastic damages are gained at the side and upper sections of the dam body. Plastic damages on the side and upper parts of the dam body are shear (n–p)

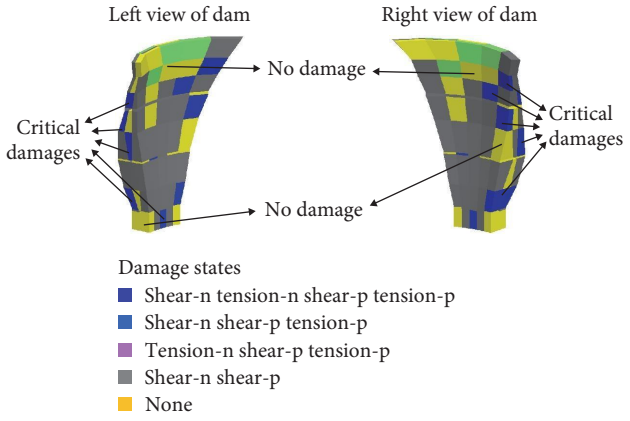

Figure 31: Earthquake damage results of the dam for Case 4.

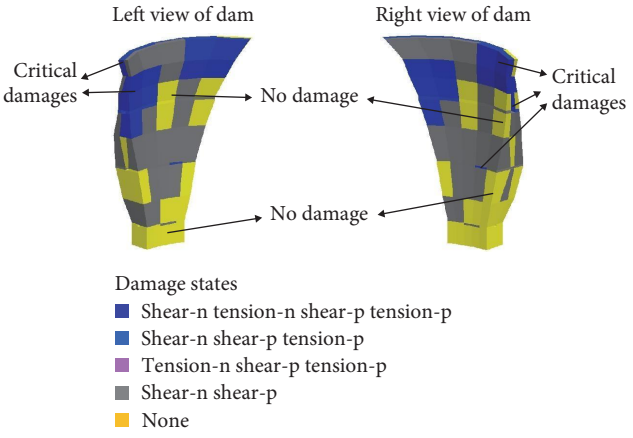

Figure 32: Earthquake damage results of the dam for Case 5.

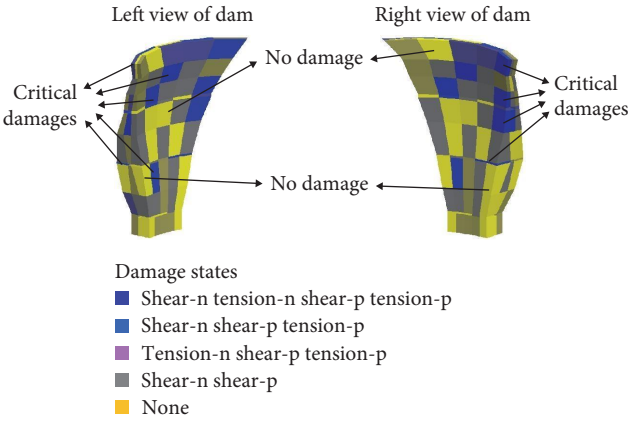

Figure 33: Earthquake damage results of the dam for Case 6.

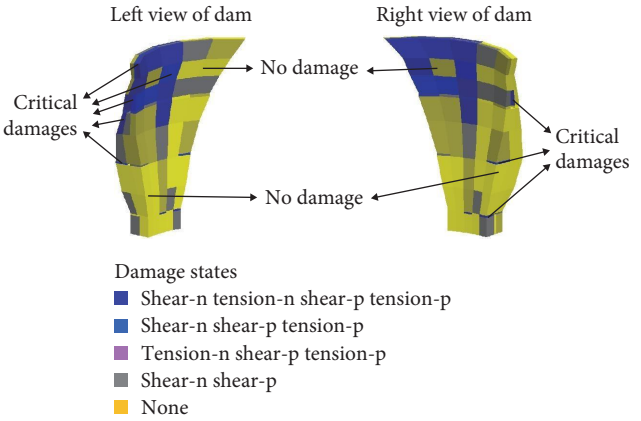

Figure 34: Earthquake damage results of the dam for Case 7.

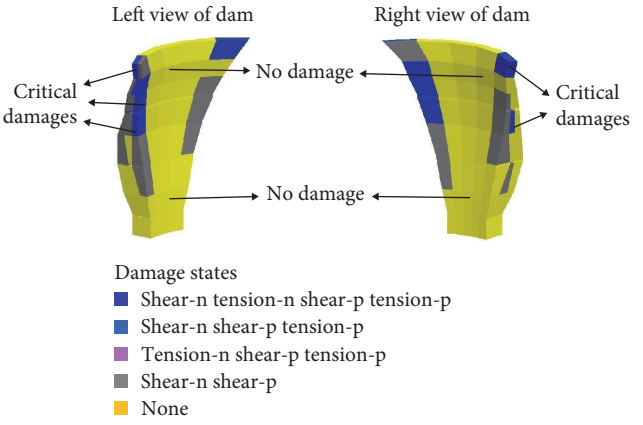

Figure 35: Earthquake damage results of the dam for Case 8.

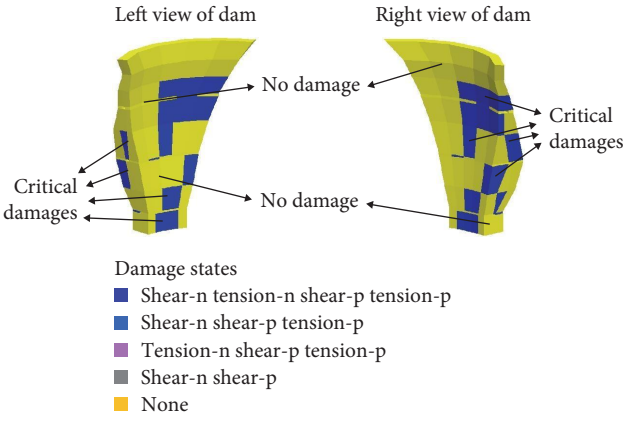

Figure 36: Earthquake damage results of the dam for Case 9.

and tension (n–p). Besides, no significant damage is observed in the lower and middle parts of the Ermenek Dam during the Case 2 earthquake. In Figure 30, the plastic damage values of the Ermenek dam are evaluated for the Case 3 earthquake. For Case 3, the plastic damages in the upper and side parts of the dam body are more critical than the lower and middle parts. Furthermore, tension (n–p) and shear (p) damages occurred in the G1 and G2 during the earthquake. But, shear (n) and tension (p) plastic damages are observed around G3 and G4. In Figure 31, the plastic damage values that occurred in the Ermenek Dam during the Case 4 earthquake are shown in detail. For Case 4, serious

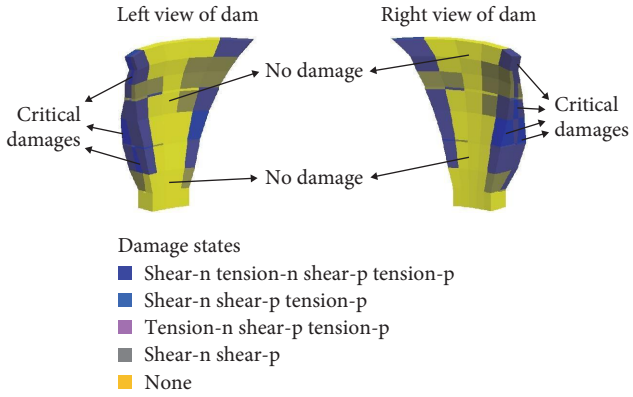

Figure 37: Earthquake damage results of the dam for Case 10.

damage is observed around the G2, G3, and G4. No significant damage is observed in the midsection of the dam body. During Case 5, shear (n–p) and tension (n–p) plastic damages took place on the side parts of the dam body, G1, and G2. No damage is observed in the lower and midsection of the dam body. Moreover, shear (n) and tension (p) are gained around G3 during Case 5 (Figure 32). During Case 6, significant damage values happened around the gallery space in the dam body (Figure 33). Shear (n–p) and tension (p) plastic damage is obtained around G1, G2, G3, and these damage values can significantly affect the structural response of the arch dams. Besides, no significant plastic damage occurred in the lower and midsections of the dam. For Case 7, shear (n–p) and tension (n–p) plastic damages are observed in the upper parts of the Ermenek Dam body and around G3. Shear (n–p) and tension (p) plastic damages are acquired in the upper sides of the dam body (Figure 34). In Figure 35, the plastic damage response of the Ermenek Dam is assessed for Case 8. For Case 8, shear (n–p) and tension (n–p) plastic damages are observed on the side parts of the dam body. Moreover, shear (n–p) and tension (p) plastic damages are acquired around G1 and G2. For Case 9, shear (n–p) and tension (n–p) plastic damages occur in the middle of the dam body and around G2, G3, and G4 (Figure 36). For Case 10, shear (n–p) and tension (n–p) plastic damages occurred at the sides of the dam body and around G1 and G3 (Figure 37). It is understood from the results obtained that during the earthquake, significant plastic damages occured not only on the sides of the dam body but also around the gallery spaces, and it is suggested that attention should be paid to the gallery space sections of the arch dams while modeling and analyzing these dams.

7. Conclusions

Investigation of the earthquake plastic damage performance of significant water structures like arch dams is crucial for the safety and sustainability of these structures. In this study, the seismic plastic damage behavior of the Ermenek Arch Dam is investigated considering the FOS analyses and the WD material model. Ermenek Arch Dam is of great importance in terms of both irrigation and electricity needs in Turkey. The following results are acquired as a result of the earthquake failure analyses of the Ermenek Dam:

(i) The proximity of the East Anatolian fault to the Ermenek Dam, which had been inactive for years, resulted in a series of major earthquakes in 2023. These earthquakes, particularly the 2023 Kahramanmaraş (Pazarcık) (Mw 7.7) and 2023 Kahramanmaraş (Elbistan) (Mw 7.6) events, caused significant seismic stress and plastic damage effects on the Ermenek Dam, surpassing the impact of other earthquakes. This highlights the critical need to investigate the seismic effects of these specific earthquakes on the dam.

(ii) During the seismic analyses, it was observed that the presence of water in the reservoir significantly influenced the dam's response. When the reservoir was full, higher principal stresses were observed in the dam body compared to the empty reservoir condition. This finding underscores the importance of considering water pressure effects when assessing the seismic behavior of arch dams.

(iii) Previous studies often employed random mesh spacing in seismic analyses of arch dams. However, this study emphasizes the necessity of a careful selection of mesh spacing. By utilizing the WD creep material model and FOS analyses, the optimal mesh spacing for the Ermenek Dam was determined to be between 5 and 25 m. This range of mesh spacing yielded FOS values above 1, signifying a desirable level of dam safety. Therefore, it is crucial to consider the most suitable mesh spacing based on thorough FOS analyses rather than adopting arbitrary choices.

(iv) The presence of gallery spaces in arch dams significantly influenced their seismic response. In the case of the Ermenek dam, which included four galleries, the analysis revealed notable accumulations of earthquake-induced principal stresses around these gallery spaces. G3 and G4 emerged as the most critical sections, exhibiting substantial stress accumulations and crack formations. Conversely, minimal principal stress values were observed around G1 and G2. These results highlight the importance of considering specific gallery spaces when assessing the dynamic response and crack behavior of arch dams.

(v) The earthquake damage analysis demonstrated that severe earthquake damage occurred on the sides of the dam body and around the gallery spaces, while minimal damage was observed in the middle and lower sections. This emphasizes the vulnerability of these areas and the need to address potential damage and reinforcement strategies.

Data Availability

The data supporting the findings of the study are available from the corresponding author upon request.

Conflicts of Interest

The authors declare that they have no conflicts of interest.

References

[1] D. Hamidian and S. M. Seyedpoor, "Shape optimal design of arch dams using an adaptive neuro-fuzzy inference system and improved particle swarm optimization," *Applied Mathematical Modelling*, vol. 34, no. 6, pp. 1574–1585, 2010.

[2] A. A. Sani and V. Lotfi, "Dynamic analysis of concrete arch dams by ideal-coupled modal approach," *Engineering Structures*, vol. 32, no. 5, pp. 1377–1383, 2010.

[3] A. Bayraktar, B. Sevim, and A. C. Altunişik, "Finite element model updating effects on nonlinear seismic response of arch dam–reservoir–foundation systems," *Finite Elements in Analysis and Design*, vol. 47, no. 2, pp. 85–97, 2011.

[4] M. Alembagheri and M. Ghaemian, "Damage assessment of a concrete arch dam through nonlinear incremental dynamic analysis," *Soil Dynamic and Earthquake Engineering*, vol. 44, pp. 127–137, 2013.

[5] J.-T. Wang, D.-D. Lv, F. Jin, and C.-H. Zhang, "Earthquake damage analysis of arch dams considering dam–water–foundation interaction," *Soil Dynamics and Earthquake Engineering*, vol. 49, pp. 64–74, 2013.

[6] R. Tarinejad, R. Fatehi, and R. S. Harichandran, "Response of an arch dam to non-uniform excitation generated by a seismic wave scattering model," *Soil Dynamics and Earthquake Engineering*, vol. 52, pp. 40–54, 2013.

[7] M. A. Hariri-Ardebili and M. R. Kianoush, "Integrative seismic safety evaluation of a high concrete arch dam," *Soil Dynamics and Earthquake Engineering*, vol. 67, pp. 85–101, 2014.

[8] Q.-L. Zhang, D.-Y. Li, F. Wang, and B. Li, "Numerical simulation of non-linear structural responses of an arch dam to and underwater explosion," *Engineering Failure Analysis*, vol. 91, pp. 72–91, 2018.

[9] J.-T. Wang, M.-X. Zhang, A.-J. Yin, and C.-H. Zhang, "Seismic fragility of arch dams based on damage analysis," *Soil Dynamics and Earthquake Engineering*, vol. 109, pp. 58–68, 2018.

[10] T. Ma, Z. Feng, C. Tang, P. Lin, and K. P. Yadav, "Overall stability analysis of Xiluodu high arch dam based on fine three-dimension numerical modeling," *Advances in Civil Engineering*, vol. 2021, Article ID 6641974, 15 pages, 2021.

[11] X. Du, Y. Zhang, and B. Zhang, "Nonlinear seismic response analysis of arch dam–foundation systems—Part I dam–foundation rock interaction," *Bulletin of Earthquake Engineering*, vol. 5, pp. 105–119, 2007.

[12] M. Wieland and G. F. Kirchen, "Long-term dam safety monitoring of Punt dal Gall Arch Dam in Switzerland," *Frontiers of Structural and Civil Engineering*, vol. 6, pp. 76–83, 2012.

[13] Z. Song, Y. Liu, and Q. Yang, "Experimental and numerical investigation on the stability of a high arch dam with typical problems of nonsymmetry: Baihetan Dam, China," *Bulletin of Engineering Geology and the Environment*, vol. 75, pp. 1555–1570, 2016.

[14] D. Zelin, W. Qianqian, and W. Jing, "Analysis on stability of an arch dam with interlayer shear zones," *KSCE Journal of Civil Engineering*, vol. 20, pp. 2262–2269, 2016.

[15] J. Chen, L. Qin, Q. Xu, and J. Li, "Seismic damage indexes of a high arch dam based on the monolith," *KSCE Journal of Civil Engineering*, vol. 24, pp. 2063–2077, 2020.

[16] J. Zhang and L. Zhang, "Analysis of seismic disaster failure mechanism and dam-break simulation of high arch dam," *Earthquake Engineering and Engineering Vibration*, vol. 13, pp. 327–335, 2014.

[17] C. Fu, X. Yao, T. Li, H. Shen, Z. Wang, and J. Jiang, "Investigation and evaluation of increasing uplift pressure in an arch dam: a case study of the Huaguangtan Dam," *KSCE Journal of Civil Engineering*, vol. 18, pp. 1858–1867, 2014.

[18] J. Pan, Y. Xu, F. Jin, and J. Wang, "Seismic stability assessment of an arch dam–foundation system," *Earthquake Engineering and Engineering Vibration*, vol. 14, pp. 517–526, 2015.

[19] D. Luo, P. Lin, Q. Li, D. Zhang, and H. Liu, "Effect of the impounding process on the overall stability of a high arch dam: a case study of the Xiluodu Dam China," *Arabian Journal of Geosciences*, vol. 8, pp. 9023–9041, 2015.

[20] Y. Chen, L. Zhang, J. Chen, C. Li, and C. Hu, "Cracking similarity simulation of induced joints and its application in model test of a RCC arch dam," *KSCE Journal of Civil Engineering*, vol. 15, pp. 327–335, 2011.

[21] E. Zacchei, J. L. Molina, and R. M. L. Rebello da Fonseca Brasil, "Seismic hazard assessment of arch dams via dynamic modelling: an application to the rules dam in granada, SE Spain," *International Journal of Civil Engineering*, vol. 17, pp. 323–332, 2019.

[22] S. Alcay, C. O. Yigit, C. Inal, and A. Ceylan, "Analysis of displacement response of the Ermenek Dam monitored by an integrated geodetic and pendulum system," *International Journal of Civil Engineering*, vol. 16, pp. 1279–1291, 2018.

[23] J.-T. Wang, F. Jin, and C.-H. Zhang, "Nonlinear seismic response analysis of high arch dams to spatially-varying ground motions," *International Journal of Civil Engineering*, vol. 17, pp. 487–493, 2019.

[24] A. Pirooznia and A. J. Moradloo, "Seismic fracture analysis of concrete arch dams incorporating the loading rate dependent size effect of concrete," *Structural Engineering and Mechanics*, vol. 79, no. 2, pp. 169–198, 2021.

[25] B. Wu, J. Niu, H. Su, M. Yang, Z. Wu, and X. Cui, "An approach for deformation modulus mechanicsm of super-high arch dams," *Structural Engineering and Mechanics*, vol. 69, no. 5, pp. 557–566, 2019.

[26] Itasca, Inc, *FLAC Version 5 User Manual*, Itasca Consulting Group Inc., Minneapolis, USA, 2002.

[27] DSI, *General Directorate of State Hydraulic Works*, DSI, Ankara, Türkiye, 2023.

[28] "Google Earth explore google earth," 2023, https://earth.google.com/web/.

[29] "Quake in Turkey highlights the hazard in the East Bay," 2020, https://seismo.berkeley.edu/blog/2020/01/26/quake-in-turkey-highlights-the-hazard-in-the-east-bay.html.

[30] AFAD, *Disaster and Emergency Management Presidency*, AFAD, Ankara, Türkiye, 2023.

[31] M. Cavuslu, "Evaluating the relationship between reservoir level changes and earthquake damage responses of high arch dams: a 3D numerical study of Ermenek Arch Dam (220 m) in Turkey," *Advances in Civil Engineering*, vol. 2023, Article ID 8944853, 22 pages, 2023.

[32] M. Karalar and M. Cavuslu, "Determination of 3D near fault seismic behaviour of Oroville earth fill dam using burger material model and free field-quiet boundary conditions," *Mathematical and Computer Modelling of Dynamical Systems*, vol. 28, no. 1, pp. 55–77, 2022.